Size and shape dependence of the magnetic ordering temperature in nanoscale magnetic particles

V. P. Shcherbakov,[1] K. Fabian,[2] N. K. Sycheva[1] and S. A. McEnroe[3]

[1] *Geophysical Observatory 'Borok' of Russian Academy of Sciences, Borok, Yaroslvaskaya oblast, 152742, Russia. E-mail: shcherb@borok.yar.ru*
[2] *Geological Survey of Norway, Leiv Erikssons vei N-7491, Trondheim, Norway*
[3] *Department of Geology and Mineral Resources Engineering, NTNU, Trondheim, Norway*

SUMMARY

Natural rocks and synthetic analogues can contain extremely small scaled magnetic minerals varying in shape from approximately equidimensional nanoparticles to lower dimensionally shaped lamellae resembling thin films or whiskers.

The magnetic ordering temperatures of such nanomagnetic structures can significantly depend on their size and shape. Here, a general method for detailed numerical or analytical calculations of these ordering temperatures is developed. Based on a modified mean-field approach, the result proves a refined version of a known scaling law that links atomic-layer number to the Curie temperatures of nanostructures. An analytic expression for the dependence of the Curie temperature on the atomic-layer number is obtained for thin films and rectangular nanostructures. It is confirmed by comparison to experimental results.

Key words: Biogenic magnetic minerals; Environmental magnetism; Magnetic and electrical properties; Magnetic mineralogy and petrology; Rock and mineral magnetism.

1 INTRODUCTION

Detailed knowledge of grain-size dependent magnetic characteristics is an essential prerequisite for rock magnetic studies. In particular, the superparamagnetic, submicroscopically fine ferrimagnetic fraction provides important palaeoclimatic and environmental information (Evans & Heller 2003), but also is an important indicator of remanence stability in rocks. As shown by Robinson *et al.* (2002), fine-scale exsolution leads to appearance of nanoscale magnetic moments, or the so-called lamellar magnetism which is responsible for the very stable natural magnetic remanence (NRM) found in rocks bearing hemoilmenties. The origin of this type of magnetism is an imbalance moment resulting from uncompensated moments of the antiferromagnetic lattice, for example, haematite grains embedded in the ilmenite matrix.

The surface-to-volume ratio is overwhelmingly larger in ultrafine than in coarse grains. Surface effects therefore considerably influence the magnetic order of ferromagnetic nanostructures, where the missing outside neighbours of the surface ions weaken the exchange coupling. As a consequence, the intensity of the spontaneous magnetization $\mathbf{M}_s$ increases from the surface to the centre of a sufficiently small nanoparticle. This phenomenon is most prominent in the vicinity of the bulk Curie temperature T_c, where exchange interactions are comparable to thermal fluctuations, and the missing boundary bonds can lead to a considerable spatial variation of $\mathbf{M}_s$, and also to a lowering of the ordering temperature in very fine particles and thin films with respect to the bulk T_c.

The quantitative details of the above effects depend on size and shape of the nanostructures, as well as on the atomic coordination number of the neighbours missing on the surface. A spatial variation of $\mathbf{M}_s$, and the decrease of T_c considerably influences results of strong field magnetization measurements and determinations of T_c in natural rocks containing such ferromagnetic nanostructures like thin films, fine-scale exsolution patterns or nanometer size particles.

The decrease of ordering temperature with size is described by the scaling law of Fisher & Barber (1972), which links the number of atomic layers N_t to the relative decrease in Curie temperature T_c according to $\frac{T_c - T_c(N_t)}{T_c} = C N_t^{-\lambda}$, where T_c is the Curie temperature of the bulk material, C is a constant and λ is the so-called 'shift exponent'. This law is based on the physical consideration that the smallest dimension of a magnetically ordered structure has to be larger than the magnetic spatial-response correlation length ξ, which describes the length scale over which a mean spin deflection influences the mean position of the neighbouring spins. Otherwise, local fluctuations influence the whole structure.

Because ξ increases with temperature as $\xi \propto [\frac{T_c}{T_c - T}]^\nu$, where ν is a critical exponent, the onset of ordering should occur when $N_t a_0 \approx \xi$, where a_0 denotes the typical distance between adjacent atomic layers. Thereby, one directly obtains $\frac{T_c - T_c(N_t)}{T_c} = C N_t^{-1/\nu}$, that is, the scaling law with $\lambda = 1/\nu$ and the fitting constant C.

For thin films, the theory of T_c reduction is based on numerical calculations, performed either using a mean-field approximation (MFA), or Green's function theory applied to a finite number of ions (Jensen & Bennemann 2006).

Here we apply Ginzburg–Landau (GL) theory, which is a natural extension of the MFA, to investigate the variation of ordering temperature, and the spatial distribution $M_s(\mathbf{r},T)$ for nanometer-scale ferromagnetic grains of various shape by assuming a smooth variation of $\mathbf{M}_s$ over the volume. This approach was previously used to study the spatial distribution $M_s(\mathbf{r},T)$ inside domain walls near the Curie temperature (Bulaevsky & Ginzburg 1963). Later, the GL energy functional was used to determine the onset of phase transition in superlattices (Wang & Mills 1992). An important advantage of the GL approach is that in several important cases it yields analytical instead of numerical solutions for both, the ferromagnetic ordering temperature and the spatial variation of the intensity $M_s(\mathbf{r},T)$. Based on these analytical solutions, it is even possible to formally 'prove' the validity of the scaling law for $N_t \gg 1$.

However, because GL theory largely neglects spatio-temporal correlations of the thermofluctuations even close to the Curie temperature, where they become relevant, it tends to predict a too small decrease in T_c. The correction needed to improve the agreement between GL theory and experiments is discussed in Section 3.

2 FREE ENERGY DENSITY IN THE GL

The free-energy density of a ferromagnet according to GL theory, is

$$F(\mathbf{r}, t) = \frac{A}{2}\mathrm{grad}^2\mathbf{m} - \frac{at}{2}m^2 + \frac{b}{4}m^4 + E_{an}(\mathbf{m}), \qquad (1)$$

where $\mathbf{m}(\mathbf{r},t) = M_s(\mathbf{r},T)/M_{s0}$ is the local spontaneous magnetization, $M_{s0} = M_s(0\,\mathrm{K})$, A is an average exchange constant and $E_{an}(\mathbf{m}) = K_{an}\,f(\mathbf{m})$ is the magnetocrystalline anisotropy energy, where $f(\mathbf{m})$ is a normalized function, invariant under the local magnetic symmetry group, K_{an} is the magnetocrystalline anisotropy constant, a and b are positive constant energy densities and $t = (T_c - T)/T_c$ is the reduced temperature measured as the distance from the Curie point T_c. The values of A, a and b are assumed to be independent of temperature.

For large structures it is possible to separate the variation of the absolute length $m(\mathbf{r},t)$, from the rotation of the vector $\mathbf{m}(\mathbf{r},t)$. In this approximation (1) splits into two independent equations for absolute value m and direction $\mathbf{m}$:

$$F_L = -\frac{at}{2}m^2 + \frac{b}{4}m^4; \qquad (2a)$$

$$F_{DW} = \frac{A}{2}\mathrm{grad}^2\mathbf{m} + E_{an}(\mathbf{m}). \qquad (2b)$$

Eq. (2a) corresponds to the Landau theory of second-order phase transitions, and minimization of (2a) determines the absolute value of $\mathbf{m}$ as $m_0(t) = \sqrt{\frac{at}{b}}$. Minimization of eq. (2b) describes spatial changes of $\mathbf{m}$ that occur on the length scale of the characteristic domain wall (DW) width $d_{DW} = \sqrt{A/K_{an}}$.

It was first noted by Bulaevsky & Ginzburg (1963) that in the vicinity of Curie temperature T_c the hierarchy of terms in (1) might be different if at $T \to T_c$ the magnetocrystalline anisotropy energy E_{an} decays slower than the Landau free energy (2a). In this case the structure of the DW may differ strikingly from the Bloch wall, because the intensity m instead of the direction of $\mathbf{m}$ changes throughout the DW.

Variations in the intensity m are also important when the space for a directional change of the vector $\mathbf{m}$ is restricted in at least one dimension, such that the minimal size of the grain $2L \ll d_{DW}$.

Therefore, variations in m are important for ferromagnetic structures resembling thin films, nanowires and nanoparticles. In these cases the surface ions have less interatomic interactions than the ions in the interior. At elevated temperatures the intensity of magnetization of the surface layers can be considerably less than the bulk magnetization value m_0, whereas the interior magnetization already may be close to m_0. Although this behaviour is always present as a surface effect, only in the case of $2L \ll d_{DW}$ it notably influences the overall magnetization and ordering temperature.

The problem of variable intensity m was studied by Wang & Mills (1992) for an alternating sequence of ferromagnetic thin films having exchange interaction at the boundaries. They solved it by using numerical solutions of the Euler equation derived from the minimization of the GL free energy density (1).

In this study we develop an analytical solution for the Euler equation describing the variable magnetization across a thin film up to T_c, and a numerical model for the magnetization variation of m in fine spherical and cubic particles up to T_c.

3 EULER EQUATION FOR THIN FILMS

A complete analytical solution can be developed for thin films or very thin 2-D lamellae, where the magnetization $\mathbf{m}(x)$, $x \in (-L, L)$, changes across the thin direction. The total number N_t of atomic layers in the film is related to the thickness $2L \ll d_{DW}$ by $N_t = 2L/a_0$.

For a typical atomic layer distance of $a_0 \approx 0.2$ nm, and ~100 atomic layers within a DW, such a thin film contains at most a few tens of atomic layers. Besides specifically designed synthetic thin films, also exsolution lamellae of a ferromagnetic inside a paramagnetic material are described by these assumptions.

When $\mathbf{m}$ changes across the film, the first term in (1), due to $2L \ll d_{DW}$, becomes comparable to the second and third terms, while the magnetocrystalline anisotropy energy, like the magnetostatic energy, remain negligible. Thus directional changes of $\mathbf{m}$ are negligible, and only the intensity m is assumed to change as a function of $x \in (-L, L)$. In this 1-D case the area density of the free energy is

$$F(T) = 2\int_0^L \left[\frac{A}{2}\left(\frac{\mathrm{d}m}{\mathrm{d}x}\right)^2 - \frac{at}{2}m^2 + \frac{b}{4}m^4\right]\mathrm{d}x. \qquad (3)$$

Due to the assumed symmetry $m(x) = m(-x)$, it is sufficient to consider only the interval $x \in (0, L)$. The Euler equation for the variational problem of minimizing (3) is

$$\xi^2\frac{\mathrm{d}^2u}{\mathrm{d}x^2} + u - u^3 = 0, \qquad (4)$$

Where $u = m/m_0$, so the range of variations of u at any given temperature t is [0,1].

The characteristic length scale

$$\xi = \sqrt{\frac{A}{at}} \qquad (5)$$

is the correlation length in the GL approximation (e.g. Fischer & Hertz 1991). Its dependence on t determines the critical exponent $\nu = \frac{1}{2}$, corresponding to the scaling exponent $\lambda = 2$. The boundary condition for m at the outer surface $x = L$ requires $m(L + a_0) = 0$, or $m + a_0\frac{\mathrm{d}m}{\mathrm{d}x} = 0|_{x=L}$. This condition is equivalent to that used Wang & Mills (1992) for the case of zero exchange interaction with the outer layer. Setting the length unit $a_0 = 1$ transforms x and ξ into dimensionless lengths, and after normalizing

the energy densities F, $a_0^3 K_{an}$, $a_0 A$, $a_0^3 a$ and $a_0^3 b$ to $k_B T_c$, where k_B is the Boltzmann constant, the free energy (1) also becomes dimensionless.

The boundary conditions for the inner and outer boundaries thereby become

$$\left.\frac{du}{dx}\right|_{x=0} = 0, \qquad \left.\frac{du}{dx}\right|_{x=N} = -u, \tag{6}$$

Where $N = N_t/2 = L/a_0$ and the inner boundary condition reflects the assumed mirror symmetry. After multiplication by du/dx, eq. (4) can be integrated, leading to a constant potential

$$E = \xi^2 \left(\frac{du}{dx}\right)^2 + u^2 - \frac{1}{2}u^4. \tag{7}$$

At $x = 0$ and $x = N$ the boundary conditions (6) yield the relations

$$E = \gamma^2 - \frac{\gamma^4}{2}, \tag{8}$$

$$(1 + \xi^2)\beta^2 - \frac{\beta^4}{2} = \gamma^2 - \frac{\gamma^4}{2}, \tag{9}$$

where $\gamma = u(0)$, $\beta = u(N)$.

Together with these relations, the differential eq. (7) has the complete analytical integral, implicitly given by

$$\begin{aligned}\frac{x}{\xi} &= \int_u^\gamma \frac{d\tilde{u}}{\sqrt{\gamma^2 - \frac{\gamma^4}{2} - \tilde{u}^2 + \frac{\tilde{u}^4}{2}}} \\ &= \sqrt{\frac{2}{2-\gamma^2}} \left\{ K\left(\frac{\gamma}{\sqrt{2-\gamma^2}}\right) - F\left[\arcsin(u/\gamma), \frac{\gamma}{\sqrt{2-\gamma^2}}\right] \right\}, \end{aligned} \tag{10}$$

where $F(\varphi, k) = \int_0^\varphi \frac{d\tilde{\varphi}}{\sqrt{1 - k^2 \sin^2 \tilde{\varphi}}}$ is the incomplete elliptic integral of the first kind, and $K(k) = F(\pi/2, k)$ is the corresponding complete elliptic integral. Using the definition of F, the last term in (10) can be written as $F[\arcsin(u/\gamma), \frac{\gamma}{\sqrt{2-\gamma^2}}] = \int_0^{\arcsin(u/\gamma)} \frac{d\varphi}{\sqrt{1 - \frac{\gamma^2}{2-\gamma^2}\sin^2\varphi}}$, such that the implicit representation of u in (10) can be transformed to the explicit solution

$$u(x) = \gamma \, sn\left[K\left(\frac{\gamma}{\sqrt{2-\gamma^2}}\right) - \frac{x\sqrt{2-\gamma^2}}{\sqrt{2}\xi}, \frac{\gamma^2}{2-\gamma^2}\right], \tag{11}$$

where the Jacobi's elliptic function $sn(z, k)$ is the inverse of $F(\varphi, k)$. Eq. (11) completely determines the magnetization profile in terms of the correlation length ξ, and the central magnetization $\gamma = u(0)$.

From (9), (6) and (10) we find the following relationships between the number of layers N, the intensity of magnetization γ in the centre and the intensity of magnetization β on the boundary:

$$\beta = \sqrt{1 + \xi^2 - \sqrt{\xi^4 + 2\xi^2 + (\gamma^2 - 1)^2}]}, \tag{12}$$

$$\frac{N}{\xi} = \sqrt{\frac{2}{2-\gamma^2}} \left\{ K\left(\frac{\gamma}{\sqrt{2-\gamma^2}}\right) - F\left[\arcsin\frac{\beta}{\gamma}, \frac{\gamma}{\sqrt{2-\gamma^2}}\right] \right\}. \tag{13}$$

Near the transition temperature t_0 of the thin film, for $t \to t_0$, both magnetizations vanish, $\gamma \to 0$. Thus in the vicinity of t_0 from (12) we obtain $\gamma \approx \beta\sqrt{1 + \xi^2}$ and eq. (13) becomes

$$N/\xi \approx \pi/2 - \arctan(1/\xi), \tag{14}$$

from which the critical value ξ_c of the correlation length (ordering temperature) can be determined. Because the correlation length ξ diverges close to the bulk Curie temperature $t = 0$, one can use the approximation $\xi \gg 1$, leading to $\arctan(1/\xi) = 1/\xi$ and

$$\xi_c = \frac{N_t + 2}{\pi}. \tag{15}$$

Now with the help of (5) we have in the GL approximation for the ordering temperature $t_0 \approx \frac{A\pi^2}{a(N_t+2)^2}$.

The free energy F in the MFA is given by (A4) in the Appendix. Comparing the energy terms in (1) and the expansion (A9), one obtains explicit expressions for b and in terms of the spin quantum number S:

$$a = \frac{3S}{1+S}, \quad b = \frac{9S[1 + 2S(1+S)]}{10(1+S)^3}$$

and the ratio $A/a = z_1/z$, where z_1 is the number of neighbours in the adjacent layer. With this expression for A/a,

$$t_0 \approx \frac{z_1\pi^2}{z(N_t + 2)^2}, \tag{16}$$

which is asymptotically equivalent N_t^{-2} dependence in agreement with the scaling law prediction $\lambda = 2$.

Below we consider for the sake of simplicity only cubic structures. For the simple cubic (scc) structure $z = 6$, $z_1 = 1$, the body centred (bcc) lattice has no exchange interactions in the same layer as all nearest neighbours are located in the adjacent layers so $z_1 = 4$, $z = 8$, for the face centred (fcc) structure one obtains $z_1 = 4$, $z = 12$. Then from (16) it follows that the decrease of T_c for the same thickness of a film is the largest for the bcc structure, when

$$t_0 \approx \frac{\pi^2}{2(N_t + 2)^2}. \tag{17}$$

The dashed line in Fig. 1 shows the change in T_c, as predicted by (17) for thin films in comparison to experimental data of Li & Baberschke (1992) for Ni (111) on W(100).

While GL theory predicts $\Delta T_c/T_c$ from 1 per cent, for 30 layers to 15 per cent for 4 layers, experimental data show substantially larger deviations (Fig. 1, crosses). More similar data are reviewed in Jensen & Bennemann (2006). This difference between GL theory and real data is at least partly due to the fact that the MFA neglects the enhanced thermofluctuations near T_c and thus leads to a wrong scaling law (5) between correlation length and temperature. Indeed, while in the MFA the critical exponent is $\nu = \frac{1}{2}$, in a 3-D Heisenberg model the value $\nu \approx 0.7$ has been found, corresponding to $\lambda = 1.42$ (Pelissetto & Vicari 2002). By using the improved scaling law

$$\xi = \frac{1}{\sqrt{2}t^\nu}, \tag{18}$$

with $\nu = 0.71$, (17) becomes

$$t_0 \approx \left(\frac{\pi}{\sqrt{2}(N_t + 2)^2}\right)^\lambda, \tag{19}$$

and a much better agreement with the data can be achieved (solid line in Fig. 2). Based on this observation, in the following calculations
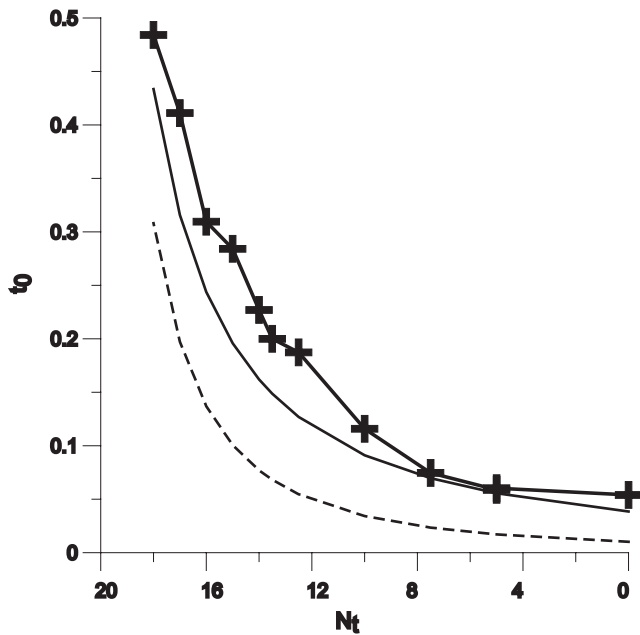
Figure 1. Relative deviation t_0 of thin-film Curie temperatures from the bulk Curie temperature as a function of thin-film layer number N_t for a film with bcc lattice. The crosses present the experimental data by Li & Baberschke 1992 for Ni (111) on W(100). The dashed line shows the GL approximation (17) while the solid line represents the corrected for the thermofluctuations dependence $t_0(N)$ (19).
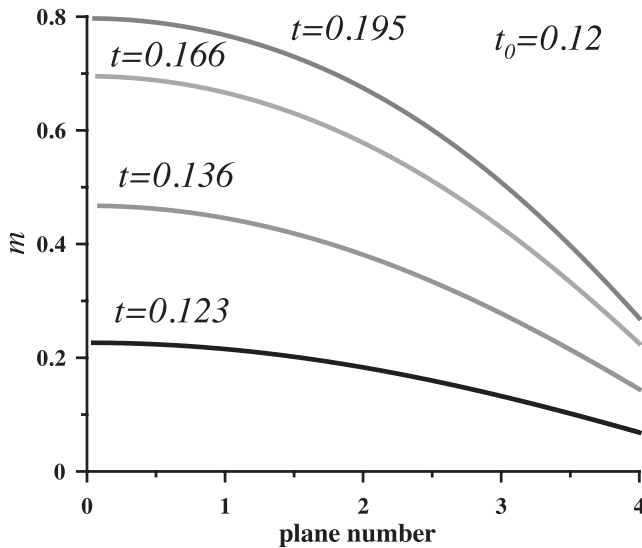

Figure 2. Magnetization versus layer number across a thin film containing $N_t = 8$ layers for different temperatures shown near the curves.

we will use (18) to translate correlation lengths into temperatures.

Fig. 2 presents the intensity of spontaneous magnetization $m = m_0 u(y)$ across a film for $N_t = 8$ according to the analytical solution (11). The threshold temperature for this N_t is $t_0 = 0.12$. The bulk magnetization $m_0 = \sqrt{at/b} = \sqrt{\frac{5(S+1)^2 t}{3[S(S+1)+1/2]}}$ was calculated in the frame of mean-field theory for $S = 5/2$.

Note that at the surface not only the magnetization is smaller, but also the increase of magnetization is much shallower than for the central moments. Indeed, near $t \cong t_0$ from (12) we have $\beta \approx \gamma/\xi$, that is, the magnetization on the boundary is about $\xi(t)$ times less than that in the centre. This drastic difference in the intensity of
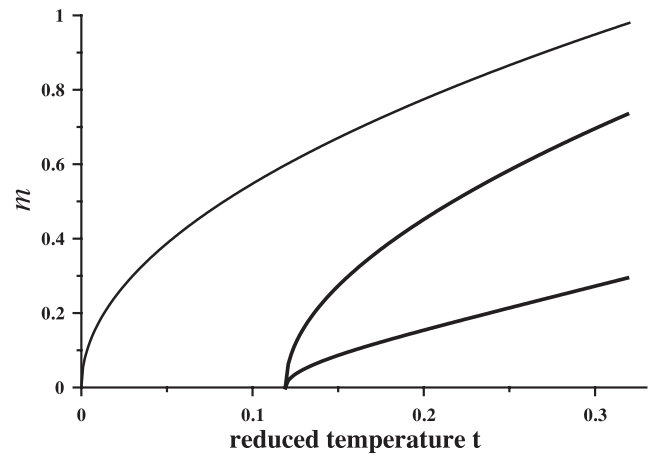
Figure 3. Comparison between the spontaneous magnetization m_0 in bcc-ordered bulk material (top curve), and a thin film with $N_t = 8$. The middle curve represents the centre, the bottom curve the surface of the thin film. All curves are plotted as a function of reduced temperature.

the magnetization in the centre and at the surface is illustrated in the Fig. 3. It shows the behaviour of spontaneous magnetization $m_0 u(y)$ in bulk material ($u \equiv 1$), in the centre and at the surface for $N_t = 8$ as a function of reduced temperature t. On cooling, the magnetization in the centre slowly approaches the bulk value, while the magnetization at the surface is still far from m_0 even at $t = 0.3$.

4 THE IN-FIELD MAGNETIZATION OF THIN FILMS NEAR T_c

The Curie temperature of natural materials is commonly determined by measurements of the strong field magnetization. To predict the temperature variation of strong field magnetization the magnetic field energy has to be added to the free energy in (3), which becomes

$$F(T) = \int_0^L \left[\frac{A}{2} \left(\frac{dm}{dx} \right)^2 - \text{sign}(t) \frac{a|t|}{2} m^2 + \frac{b}{4} m^4 - mh \right] dx, \quad (20)$$

where the magnetic field h is normalized to $k_B T_c/(\mu_0 M_s(0\,\text{K}))$, which corresponds to the molecular field in mean-field theory.

Similar to eq. (7), the functional (20) also has the potential

$$E = \xi^2 \left(\frac{du}{dx} \right)^2 + \text{sign}(t) u^2 - \frac{1}{2} u^4 - h_n u, \quad (21)$$

where

$$h_n = h \sqrt{b} \Big/ (a|t|)^{3/2}.$$

The boundary conditions (6) now yield the relations

$$E = \text{sign}(t) \gamma^2 - \frac{\gamma^4}{2} + \gamma h_n,$$

$$\left[\text{sign}(t) + \xi^2 \right] \beta^2 - \frac{\beta^4}{2} + \beta h_n = \text{sign}(t) \gamma^2 - \frac{\gamma^4}{2} + \gamma h_n. \quad (22)$$

From (20) in analogy with (10) we obtain the magnetization

$$\frac{x}{\xi} = \int_u^\gamma \frac{d\tilde{u}}{\sqrt{\text{sign}(t)(\gamma^2 - \tilde{u}^2) - \frac{\gamma^4}{2} - h_n \gamma + \frac{\tilde{u}^4}{2} + h_n \tilde{u}}}. \quad (23)$$
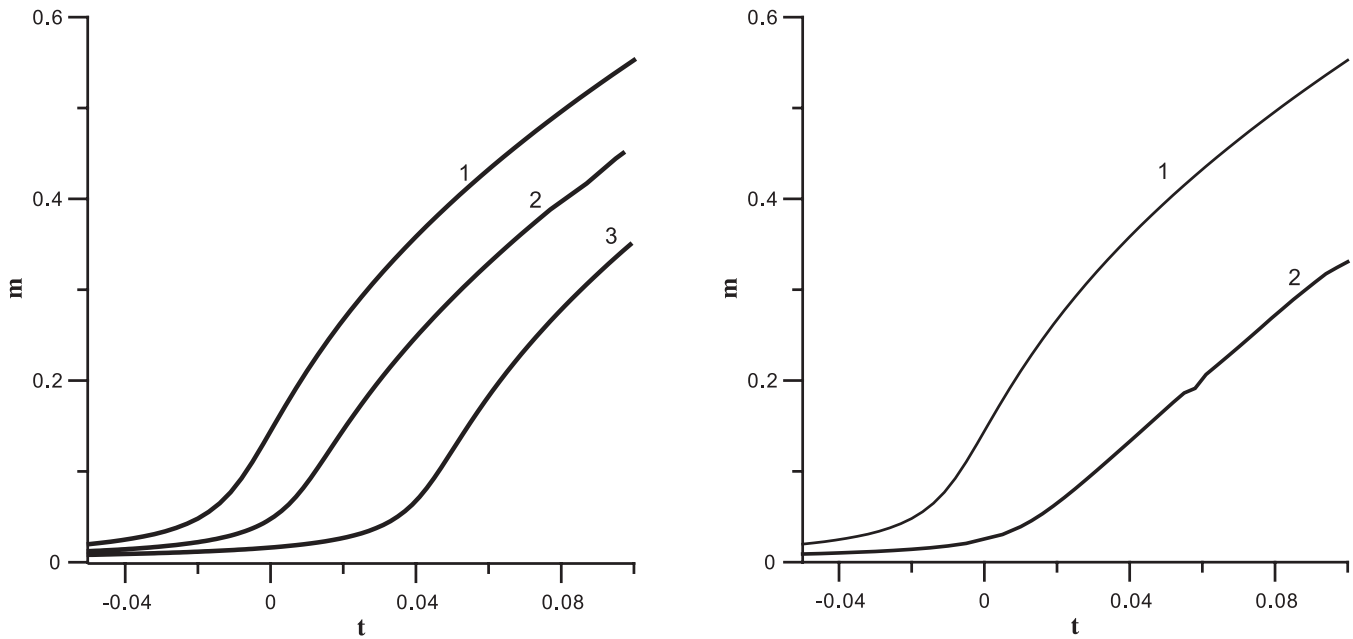
Figure 4. (a) In-field net-magnetization $m(t)$ for thin film with $N_t = 16$ (curve 3) and 40 (curve 2) at $h\sqrt{b}/a^{3/2} = 0.001$ (from right to left). (b) The curve 2 shows the sum of $m(t)$ for the collection of thin films with $N_t = 6, 8, \ldots 40$ at $h\sqrt{b}/a^{3/2} = 0.001$. For the comparison, the curve 1 in both figures presents $m_0(t)$ dependence for the bulk material.

In this case, $u(x)$ can be efficiently calculated by numerically solving the system of eqs (22) and (23). The net magnetization of the film can be then calculated simply by summation of the magnetization of the planes constituting the film. Some results of such the calculations with ξ determined by (18) are shown in Fig. 4.

Fig. 4 clearly shows that the presence of ultrafine grains considerably reduces the Curie temperature determined as the maximum of either first or second derivative in relation to t. Certainly, the character of overall $m(t)$ behaviour is pre-determined by the distribution function of total volume of films with given size N_t. In this aspect, the curve 2 in Fig. 4(b) was obtained from the suggestion that each member of the sum gives the same contribution in the resulting magnetization. In other words, it was suggested that the number of films with given size is inverse in N_t. As is seen, a distinctive feature of this case is that the increase $m(t)$ right below the Curie point $t = 0$ is quite smoothed so that dm/dt is almost constant in the vicinity of T_c.

4 MAGNETIZATION OF RECTANGULAR NANOPARTICLES UP TO T_c

We now turn from thin films towards 3-D nanoparticles. The 3-D analogue of eq. (4) is

$$\xi^2 \Delta u + u - u^3 = 0, \qquad (24)$$

where Δ is the Laplace operator (3-D grains). For a cubic structure it is natural to consider a rectangular nanoparticle with the sizes $N_{tx} = 2N_x$, $N_{ty} = 2N_y$ and $N_{tz} = 2N_z$. The reduced transition temperature t_0 can be found again from the linearized eq. (24) $\xi^2 \Delta u + u = 0$, which in the Cartesian coordinates has the solution

$$u = \gamma \cos \frac{k_x x}{\xi} \cos \frac{k_y y}{\xi} \cos \frac{k_z z}{\xi} \qquad (25)$$

with the condition

$$k_x^2 + k_y^2 + k_z^2 = 1. \qquad (26)$$

Remind that the constant γ in (25) is the magnetization in the centre of the grain.

The boundary conditions are $\cdot \frac{du}{dx}|_{N_x} = \frac{du}{dy}|_{N_y} = \frac{du}{dz}|_{N_z} = -u$ or

$$\cot \frac{k_x N_x}{\xi} = \frac{k_x}{\xi}, \quad \cot \frac{k_y N_y}{\xi} = \frac{k_y}{\xi}, \quad \cot \frac{k_z N_z}{\xi} = \frac{k_z}{\xi}. \qquad (27)$$

From (26) and (27) we obtain the coefficients k_x, k_y and k_z as well as the critical correlation length ξ. Using the inequality $\xi \gg 1$, so that $\arctan \frac{k_x N_x}{\xi} = \frac{k_x}{\xi}$ and so on, we find instead of (27) $\frac{k_x(N_x+1)}{\xi} \approx \frac{\pi}{2}$, etc. Now accounting for (26) obtain

$$\xi_c^{-2} = \pi^2 \left[\frac{1}{(N_{tx} + 2)^2} + \frac{1}{(N_{ty} + 2)^2} + \frac{1}{(N_{tz} + 2)^2} \right], \qquad (28)$$

which is exactly three times more than the square of the critical correlation length for thin film of the same size N_t. For a long whisker it is twice the reduction for a thin film. Accordingly, the ordering temperature in a cube in analogy with (19) is

$$t_0 \approx \left(\frac{\sqrt{3}\pi}{\sqrt{2}(N_t + 2)} \right)^\lambda. \qquad (29)$$

The internal magnetic structure of a cubic particle is truly 3-D. To visualize it, numerical modelling using the MFA was used assuming that the order parameter m_i of the ith ion with spin S obeys the eq. (A11) from the Appendix

$$m_i = B_S \left[\frac{3S \sum_j m_j}{2z(1 + S)} \frac{T_c}{T} \right], \qquad (30)$$

where B_s is the Brilluoin function and the sum in (30) must be performed over the set NN_i of nearest neighbours of the ith ion. The structure is here calculated for ions with spin quantum number $S = 5/2$.
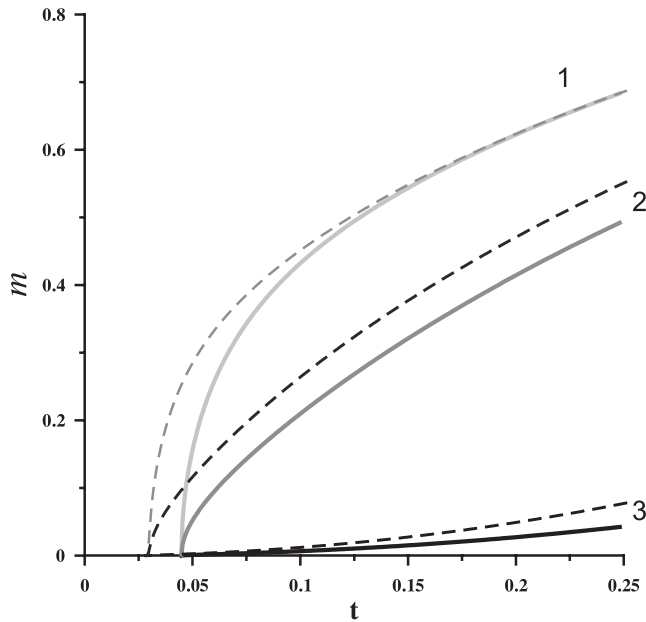
Figure 5. Magnetization m against the reduced temperature t for bcc (full lines) and fcc (dashed lines) lattices. Total number of layers in both cases is $N_t = 17$. 1—magnetization of cube vertices, 2—magnetization at cube centre, 3—total magnetization.

These numerical models are strictly valid well below the Curie temperature. Temperatures t close to t_0 must be rescaled, as for the linearized T_c calculations mentioned above. Rescaling near T_c is necessary, because the numerical calculations rely on the MFA, and do not take into account temporal correlations of the thermofluctuations. The temperatures t in Figs 5 and 6 therefore correspond to (29) with $\lambda = 2$. Accordingly, the temperatures related to the magnetic structures shown in Figs 5, 6 and later figures, which demonstrate the spatial distributions $M_s(\mathbf{r})$ must be rescaled if they are close to t_0. As in the thin film case, a first-order correction to the temperatures given in these figures can be obtained simply by renormalization $t \to t^{\lambda/2}$ with $\lambda = 1.42$ if $t/t_0 < 3$. For larger t the MFA is physically reasonable and the corresponding t values are correct in very good approximation.

Near the corners and at the edges of a cube the number of broken bonds is largest and accordingly the lowest magnetization intensity is observed in these areas in Figs 5 and 6. Quantitatively, in the corners of the body centred cube from (25) and (27) one obtains in the linear approximation

$$u(N, N, N) = \gamma \cos^3(N/\sqrt{3}\xi) \approx a\frac{\pi^3}{8N^3}, \tag{31}$$

where a is the magnetization in the centre. Similarly, on the edges $u \approx a\frac{\pi^2}{4N_t^2}$, and on faces $u \approx a\frac{\pi}{2N_t}$. In other words, if the order parameter m on faces is N times less than the value of m in the centre, it drops in the corners by a factor of N_t^3.

The magnetization cross-sections in Fig. 6(c) clearly show that slightly below the ordering temperature ($t = 0.05$) the intensity of magnetization is very inhomogeneous over the volume and has a spherically smoothed core with a periphery where the intensity is much lower in accordance with (31). On cooling, the core grows and becomes more homogeneous but the near-surface region is still weakly magnetized (Figs 6b and a).

5 DISCUSSION

The above-mentioned theoretical calculations provide a sufficiently detailed framework for using the reduction of the Curie temperature as a quantitative method to determine grain sizes of extremely small ferromagnetic minerals in natural materials.
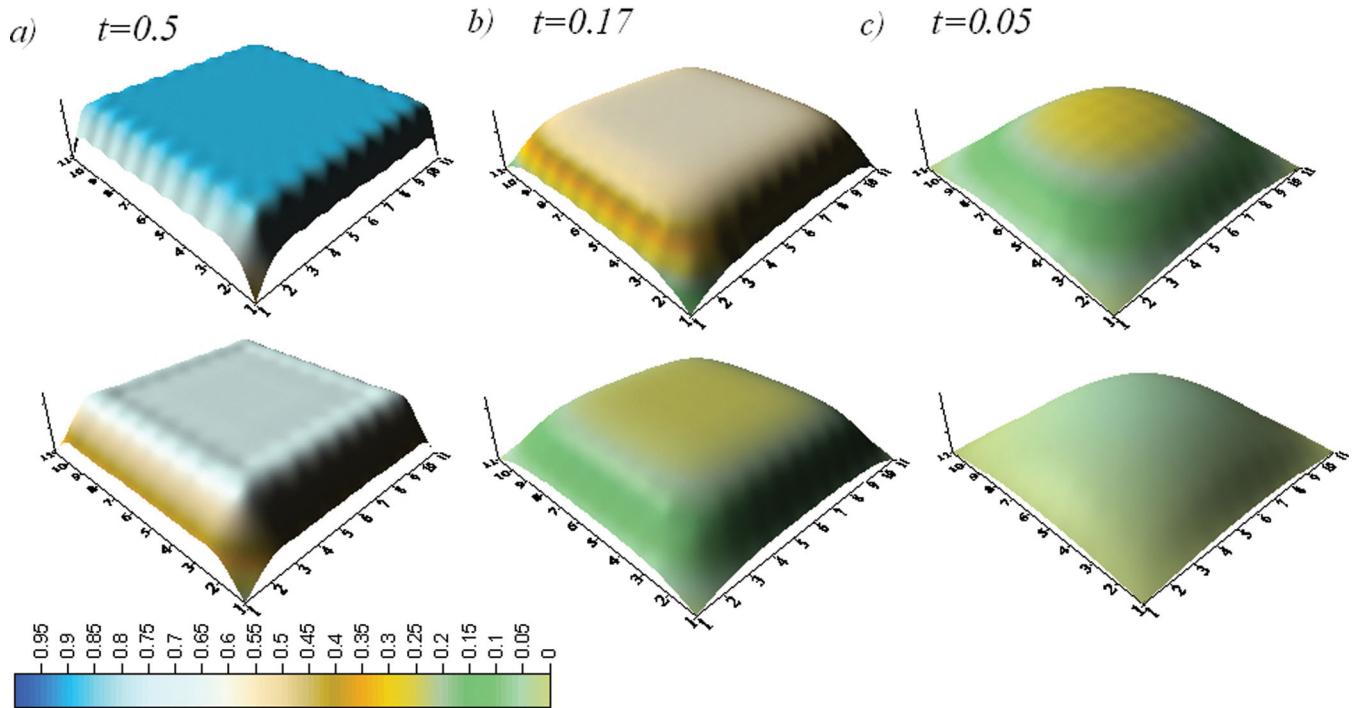

Figure 6. Numerical models of the magnetization intensity across a bcc(001) cubic nanoparticle with $N_t = 21$ layers. The top graphs in (a)–(c) show the intensity of magnetization across the central layer at the indicated temperatures t. The bottom graphs show the corresponding magnetization over the surface layer. The critical temperature for this particle is $t_0 = 0.03$. (The rescaled critical temperature is $t_0 = 0.08$.)

The main advantage of the GL approach is that it leads to analytical formulae for the Curie temperatures of thin films, whiskers and rectangular nanoparticles. A crude estimate claims that long-range ordering approximately sets in when $N_t \approx \xi$. The more detailed analysis above showed that the correct relationship between these two lengths is given by eq. (15) for a thin film, and by (28) in the more general case of a rectangular particle. In accordance with common sense, 2- or 3-D grains experience the phase transition at considerably lower temperatures than thin films of the same thickness. Because thin films can be treated as 1-D objects, their theoretical analysis is much easier, and not only the ordering temperatures but also the spatial distribution of their spontaneous magnetization can be expressed analytically. Based on the understanding of these analytical solutions it is possible to derive quantitative predictions that can be compared to experimental data and provide grain size information independent of other methods commonly used in rock magnetism.

Sadeh *et al.* (2000) studied the size dependence of T_c for a suite of magnetite nanoparticles obtained by coprecipitation (squares in Fig. 7). This bilogarithmic plot of the t_0 data as a function of nominal grain size d_{nom} shows that even rather big grains, with sizes up to 20 nm can have significantly lowered ordering temperatures. To fit these data with the quantitative scaling law (29), a reduced effective grain size d_{eff}, so that $N_t = d_{\mathrm{eff}}/a_0$, must be applied with d_{nom} by a factor 3–6 less than d_{nom}. This discrepancy probably is due to the fact that the precipitated grains consist of densely clustered smaller ones. It also could occur due to high dislocation densities or fracturing, both of which are however unlikely here. The scaling law with a reduced exponent $\lambda = 1.42$ seems to be applicable only to the smallest grain sizes $d_{\mathrm{nom}} < 10$ nm or $d_{\mathrm{eff}} < 3$ nm. Interestingly, the GL model with $\lambda = 2$ provides a reasonable fit for the whole grain size interval if some variation in $d_{\mathrm{nom}}/d_{\mathrm{eff}}$ is allowed. It should be noted that typically a pure power-law $t_0 \propto C/d^\lambda$ is fit to the data by freely adjusting C. This adjustment here is replaced by using the more rigorous law (29), which only allows for adjustments of the effective grain size, which have to be physically reasonable, for example, $1 < d_{\mathrm{nom}}/d_{\mathrm{eff}} < 10$.
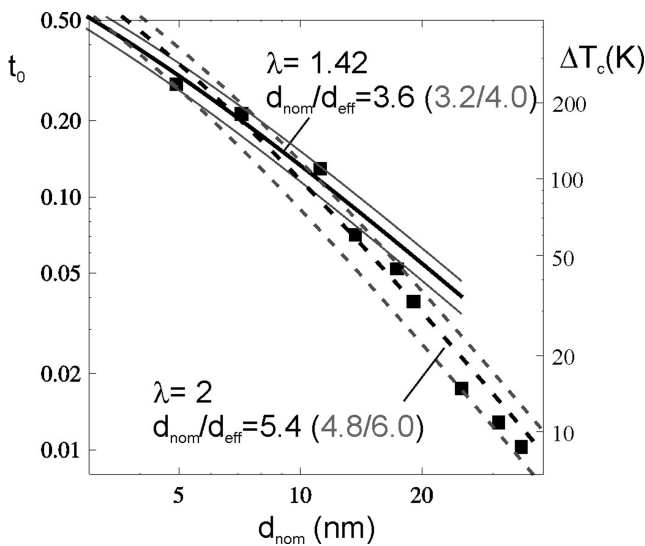
Figure 7. Experimental data of t_0 versus grain size by Sadeh *et al.* (2000) for precipitated magnetite grains (squares). The solid and dashed lines represent fits to the scaling law (29) for $\lambda = 1.42$ and $\lambda = 2$, with reduced effective grain size, which mathematically reflects clustering and fracturing.
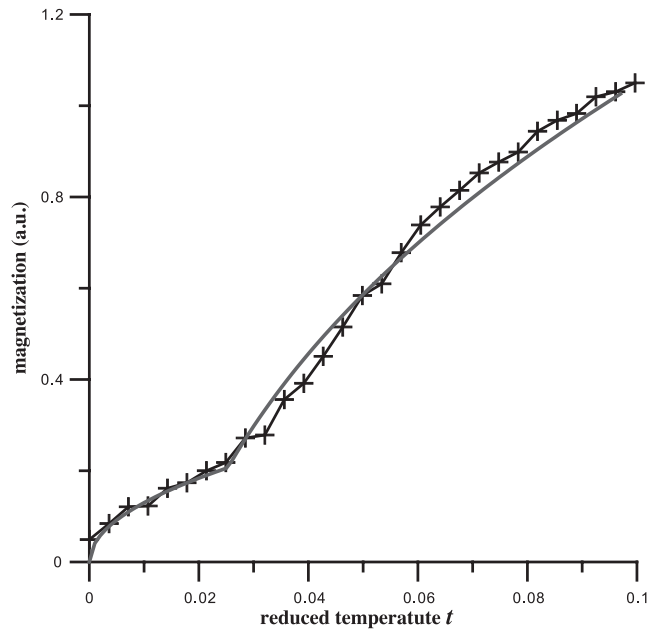
Figure 8. Crosses are the experimental data. The full line presents the curve obtained from numerical modelling of thin films (lamellae) for $\lambda = 1.42$ and the size $N_t = 22$.

A practical example of a grain size determination from an $M_s(T)$ curve comes from well-crystallized magnetite exsolution lamellae within a synthetic haematite–ilmenite solid solution containing nominally 40 per cent ilmenite. The weight-normalized $M_s(T)$ curve above the Ilm40 Neel temperature $T_N \sim 330\ ^\circ$C indicates that the sample contains about 0.1 per cent vol magnetite. $M_{rs}(T)$ is zero above T_N showing that the magnetite is superparamagnetic in this temperature region. Transmission electron microscope (TEM) images show sporadic well-crystallized magnetite lamellae inside the bulk Ilm40 with minimum side lengths below 10 nm (McEnroe *et al.* 2007). The normalized $M_s(T)$ curve of this sample above T_N is shown by crosses in Fig. 8.

A quantitative numerical model of these data is based on 35 per cent bulk magnetite and 65 per cent of thin lamellae, corresponding to a thickness of $N_t = 22$. The fit (solid line in Fig. 8) is calculated as the sum of 35 per cent bulk magnetization $m_0(t)$ and 65 per cent magnetization from an ensemble of thin films with $N_t = 22$ (thickness 4–5 nm). It is based on the integral of (11) from $x = 0$ to N, which gives the overall film magnetization as

$$M_t(N_t) = Ln\left\{ \frac{1 + \gamma\, sn[N(\sqrt{2(2-\gamma^2)})\xi, \frac{\gamma^2}{2-\gamma^2}]}{dn[N(\sqrt{2(2-\gamma^2)})\xi, \frac{\gamma^2}{2-\gamma^2}]} \right\} \bigg/ \sqrt{2}\xi. \quad (32)$$

Here $dn(z, k)$ is the Jacobi's elliptic function and the correlation length ξ is given by (18).

A similar grain size can be directly read from Fig. 7, when noting that the break of the measured $M_s(t)$ curve lies around $t = 0.03$, which corresponds to a nominal size of $d_{\mathrm{nom}} \approx 22$ nm in Fig. 7, which yields an effective size of $d_{\mathrm{eff}} \sim 4$–6 nm.

From a Langevin model of the 700 K hysteresis loop of this sample, an approximate average volume of $(15\ \mathrm{nm})^3$ is determined for the magnetite lamellae. Both results together imply a thin elongated or oblate lamella shape, which agrees with the TEM image in McEnroe *et al.* 2007.

A reduction of T_c due to the effect of nanosize is probably also relevant for the Yucca mountains tuffs, for which published T_c

measurements of Tiva Canyon samples show T_c around 800–825 K (Worm & Jackson 1999; Carter-Stiglitz *et al.* 2006), while the bulk T_c of magnetite is 858 K. This difference has been interpreted to indicate the presence of titanium, at about a fraction of 10 per cent ulvospinel. TEM images show that the Tiva Canyon ferromagnetic particles are of needle shape with small size 5–10 nm, thus the number of planes at across the needle is about 25–50. According to the previous calculations, their reduction of ordering temperature should be approximately $t_0 \approx (N_t + 2)^{-\lambda}$. With $\lambda = 1.42$ this gives $t_0 = 0.02$–0.05 or 15°–40° reduction from the bulk T_c of magnetite. Thus, at least part of the difference between the T_c of pure magnetite and the ordering temperature must be due to particle size.

Ferromagnetic particles below their critical size of $\sqrt{(A/K)}$ are in a single-domain state and should carry an essentially homogenous magnetization, leading to sharp nuclear gamma resonance lines. However, close to the ordering temperature, the magnetization in nanosize particles becomes inhomogeneous over the volume as is illustrated in Figs 2, 3, 5 and 6. The inhomogenity of magnetization implies that the effective field H_{eff} acting on an ion inside the particle depends on its location. The resulting broad distribution of magnetic hyperfine fields is similar to that observed in amorphous materials (Yoon *et al.* 2000; Kiss *et al.* 2011). One consequence of this is the widening of the nuclear gamma resonance lines for nanostructures at elevated temperatures. To estimate the effect, one must find the distribution function (d.f.) $f(H_{\mathrm{eff}})$. As far as the effective field of the hyperfine splitting is proportional to the local order parameter u, the d.f. $f(H_{\mathrm{eff}})$ is identical to the distribution function $f(u)$.

For a thin film, the area-density of spins is independent of the distance x from the film's middle plane. Therefore, the cumulative distribution function $n(u) = \mathrm{prob}(m/m_0 > u)$ simply becomes $n(u) = x(u)/N$, where x and u are related to each other through (10). Fig. 9 shows examples of such cumulative distribution function for a thin film containing $N_t = 40$ layers. The cumulative distribution function
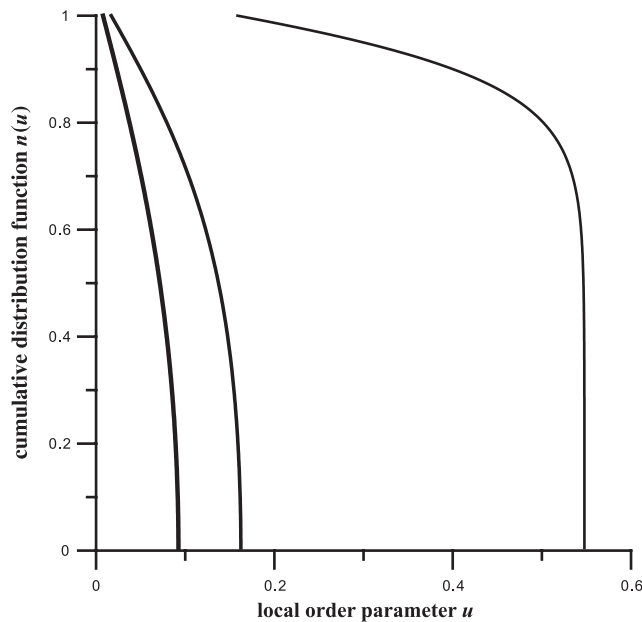
of effective fields steeply increases at the right end of the plots, due to the prevalence of fields from the almost homogeneous core, even at the temperatures close to the ordering temperature. At lower temperatures, more moments are almost perfectly ordered, and more effective fields lie near the maximum value. This leads to a steep, step-like increase of the cumulative distribution.

Figs 10 and 11 present numerically modelled cumulative histograms of y for two cubic bcc grains with $N_t = 17$ and $N_t = 37$ layers, respectively. The corresponding physical sizes are about 3.5 and 7 nm. For higher temperatures, close to the ordering temperature, one obtains a smooth distribution function with its maximum at low fields (left diagrams in Figs 10 and 11). This is especially distinct for smaller grains (Fig. 10) and reflects predominant contribution of the less-ordered peripheral volume in comparison to the better-ordered core volume.

The right-hand diagrams in Figs 10 and 11, as well as Fig. 12, show that at lower temperatures the spectra still display non-smooth behaviour. This consists of a large step at highest fields, and three additional small steps at lower fields. Note that Fig. 12 relates to a rather big grain, with $N_t = 53$ bcc(001) layers at $t = 0.76$, which corresponds to a temperature far below T_c and the size about 10 nm. Apparently, the main peak reflects the almost homogeneously magnetized core, while the intermediate ones are due to the spins situated on the faces, edges and vertices of the grain.

It is worth noting that the temperatures where the inhomogeneity of magnetization may lead to the widening of nuclear gamma-resonance lines lies in moderate and elevated temperature range as it is seen from the Figs 9–12. The effect can be notable for the grains of a few nanometres up to 20 nm size, which are usually superparamagnetic at these temperatures. Hence, in practice the observation of the widening of superfine splitting at moderate temperatures requires an application of a strong external magnetic field to suppress the superparamagnetic behaviour of the grains.

The results obtained here for ferromagnetic particles essentially remain valid also in case of antiferromagnetic particles (e.g. ilmenite and haematite). Instead of the magnetization **m**, the order parameter in this case is the antiferromagnetic vector $\mathbf{t} = (\mathbf{a}-\mathbf{b})/2$ which represents the antiparallel sublattice magnetization vectors **a** and **b**. It is also possible to extend the above-mentioned results to the more general case of ferrimagnetic particles. The main difficulty with this generalization is that a set of two Euler equations for the two ferrimagnetic sublattices would have to be solved. It is worthwhile to remind that for both titanomagnetites and haemoilmenites the exchange interactions between the sublattices are much stronger than the in-plane interactions. Thus, this case is similar to the one considered here case of the bcc lattice when half of bonds are lost on the surface. Hence, we also should expect quite strong effect of their T_c and M_s values on their size and shape. While a detailed discussion of these generalizations is beyond the scope of this paper, semi-quantitative estimations can be done on the basis of the above-mentioned results for ferromagnetic particles.

Figure 9. Plot of the cumulative distribution $n(u)$ of local order parameter u for a thin film ($t_0 = 0.015$) with $N_t = 40$ layers for temperatures $t = 0.023$, $t = 0.038$ and $t = 0.2$, from left to right).

6 CONCLUSIONS

Ultrafine magnetite particles are frequently studied in rock and environmental magnetism. They either are indicative for the formation mechanism of iron oxides or notably influence the magnetic properties of natural rocks. Characterization of this fine fraction is important, and several methods are known. Here we develop a new
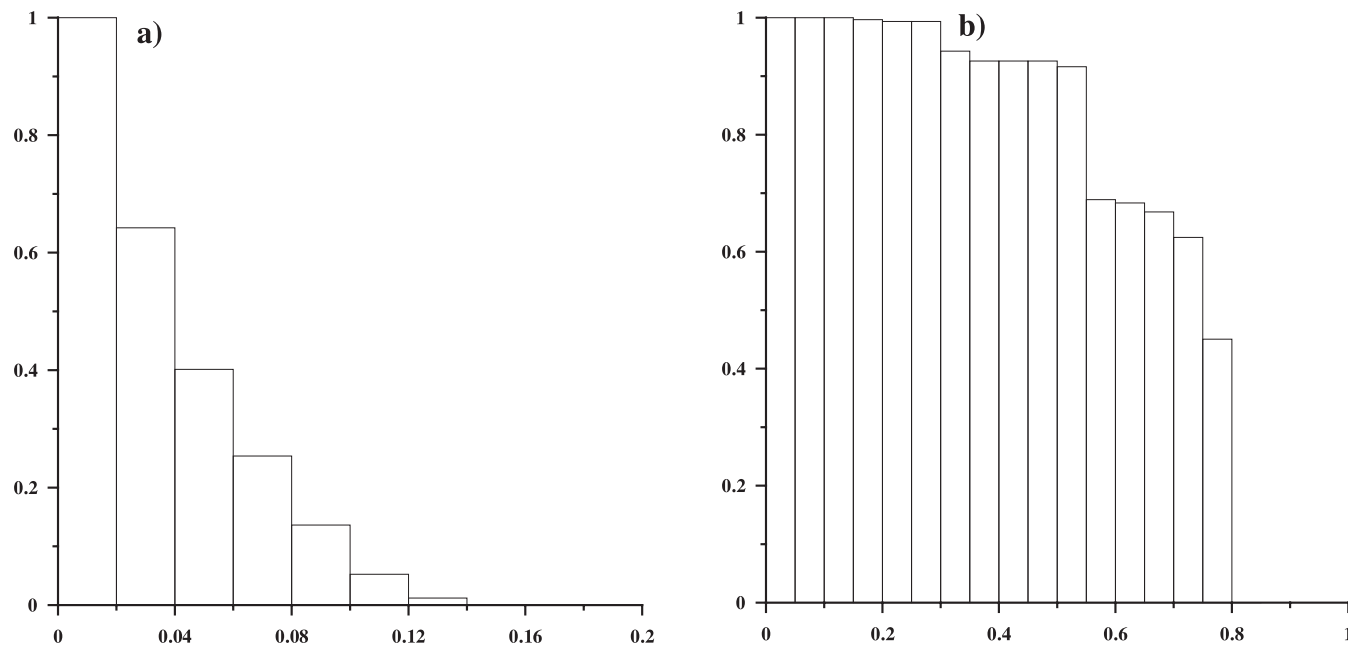
Figure 10. Cumulative distribution histograms $f(u)$ of the local order parameter u for a cubic particle with $N_t = 17$ layers at temperatures $t = 0.052$ (left-hand side), and $t = 0.33$ (right-hand side).
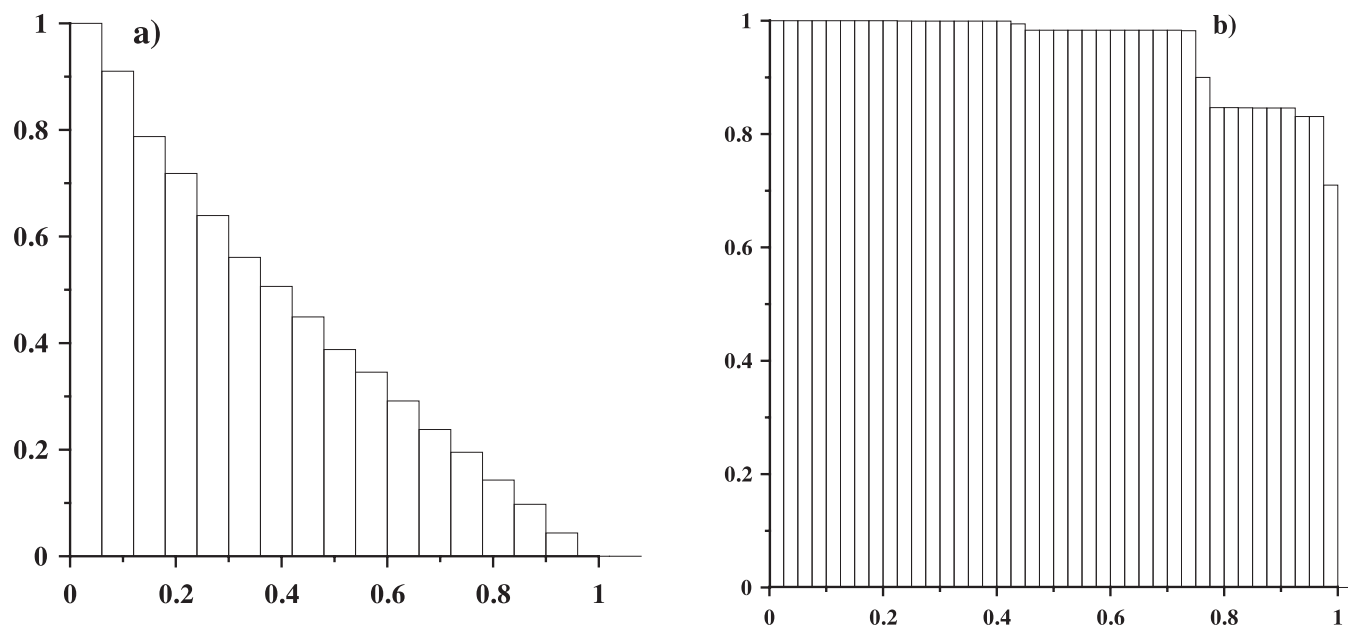

Figure 11. Cumulative distribution histograms $f(u)$ of the local order parameter u for a cubic particle with $N_t = 37$ layers ($t_0 = 0.01$) at temperatures $t = 0.02$ (left-hand side), and $t = 0.5$ (right-hand side).

quantitative approach that uses the variation of Curie temperature with grain size.

The effect is well known for nanostructures in material science, but a quantitative theory and a practical application to rock magnetism has been missing.

Based on an analytical approach, a general GL MFA is used to derive magnetic ordering temperatures and spontaneous-magnetization distributions for different classes of nanostructures, including thin films, whiskers and nanoparticles of different shapes. Analytical expressions for the ordering temperatures of these nanostructures are given. Closed-form expressions for all magnetic prop-

erties are obtained for thin films, which can be described by 1-D differential equations. A comparison to experimental data shows that the improved scaling law, derived here, better describes the ordering temperature of nanostructures than the commonly used power laws.

On a practical level, Fig. 7 provides a simple means to transfer reduced Curie temperatures for magnetite to approximate particle sizes. Quantitative calculations of spontaneous magnetization distribution functions in nanostructures contribute to the understanding of line broadening in nuclear gamma resonance in magnetic nanoparticles.
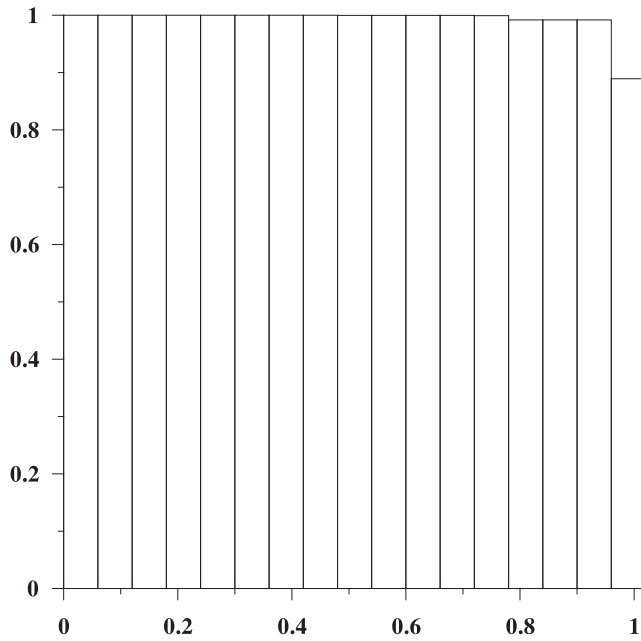
Figure 12. Cumulative distribution function $f(u)$ of the local order parameter u for a cube with bcc(001) lattice and $N_t = 53$ layers at low temperature $t = 0.76$.

REFERENCES

Bulaevsky, L.N. & Ginzburg, V.L., 1963. Temperature dependence of the shape of the domain wall in ferromagnetics and ferroelectrics, *Zh. Eksp. Teor. Fiz.,* **45,** 772–779.

Carter-Stiglitz, B.S., Solheid, P.A., Egli, R. & Chen, A.P., 2006. Tiva Canyon Tuff (II), *IRM Q.,* **16**(1), 1, 8–10, http://www.irm.umn.edu/quarterly/irmq16-1.pdf.

Evans, M. & Heller, F., 2003. *Environmental Magnetism, Principles and Applications of Enviromagnetics,* Vol. **86,** Academic Press, San Diego, CA.

Fisher, M.E. & Barber, M.N., 1972. Scaling theory for finite-size effects in the critical region, *Phys. Rev. Lett.,* **28,** 1516–1518.

Fischer, K.H. & Hertz, J.A., 1991. *Spin Glasses,* Cambridge University Press, Cambridge.

Jensen, P.J. & Bennemann, K.H., 2006. Magnetic structure of films: dependence on anisotropy and atomic morphology, *Surf. Sci. Rep.,* **61,** 129–199.

Kiss, L.F., Balogh, J., Bujdoso, L., Kaptas, D., Kemeny, T., Kovacs, A. & Vincze, I., 2011. Mössbauer study of ultrathin Fe/Al multilayer films, *J. Alloys Compd.,* **509S,** S188–S192.

Li, Y. & Baberschke, K., 1992. Dimensional crossover in ultrathin Ni(111) films on W(110), *Phys. Rev. Lett.,* **68,** 1208–1211.

McEnroe, S.A., Miyajima, N., Robinson, P., Fabian, K., Burton, B.P. & Boffa Ballaran, T., 2007. Cryptic intergrowth of magnetite-like phase in synthetic titanohematite. Annual Report, Bayerisches Geoinstitut, Universität Bayreuth, Germany.

Pelissetto, A. & Vicari, E., 2002. Critical phenomena and renormalization-group theory, *Phys. Rep.,* **368,** 549–727.

Robinson, P., Harrison, R.J., McEnroe, S.A. & Hargraves, R.B., 2002. Lamellar magnetism in the haematite-ilmenite series as an explanation for strong remanent magnetization, *Nature,* **418,** 517–520.

Sadeh, B., Doi, M., Shimizu, T. & Matsui, M.J., 2000. Dependence of the Curie temperature on the diameter of Fe_3O_4 ultra fine particles, *J. Magn. Soc. Jpn.,* **24,** 511–514.

Wang, R.W. & Mills, G.L., 1992. Onset of long-range order in superlattices: mean-field theory, *Phys. Rev.,* **46,** 11 681–11 687.

Worm, H.-U. & Jackson, M., 1999. The superparamagnetism of Yucca Mountain Tuff, *J. geophys. Res.,* **104,** 25415–25425.

Yoon, S.H., Lee, H.H., Kim, S.B., Kim, W.C. & Kim, C.S., 2000. Distributions of hyperfine parameters in amorphous $Fe_{78}A_{14}Nb_5B_{12}Cu_1$ alloys, *J. Magn. Magn. Mater.,* **215–216,** 362–364.

APPENDIX

The exchange energy of two identical interacting magnetic ions (ith and jth) in the classic Heisenberg approximation is $E_{\text{exc}} = -2J\vec{S}_i\vec{S}_j$, where J is the exchange integral. If the finite volume effect can be neglected, and only nearest neighbours are taken into account, all spins in a ferromagnetic grain are statistically identical. Let $\langle S_i \rangle$ be the time average of the spin, then the Hamiltonian of N interacting spins is

$$
\begin{aligned}
H &= \sum_{i \neq j} -J\vec{S}_i\vec{S}_j \\
&= \sum_{i \neq j} \{-J(\vec{S}_i - \langle S_i \rangle)(\vec{S}_j - \langle S_j \rangle) + J_{i,j}\langle S_i \rangle \langle S_j \rangle - 2J_{i,j}\vec{S}_i \langle S_j \rangle\}.
\end{aligned}
$$
(A1)

The MFA means the neglect of the terms of type $(\vec{S}_i - \langle S_i \rangle)(\vec{S}_j - \langle S_j \rangle)$, which describe the temporal correlations between spins. Then the statistical sum $Z = \sum \exp \frac{-H}{k_B T}$, where the summation must be done over all possible configurations, reduces to

$$
Z = \exp\left(\frac{-\sum_{i \neq j} J\langle S_i \rangle \langle S_j \rangle}{k_B T}\right) \prod_{i=1}^{N} \sum_{n=-S}^{S} \exp \frac{n\sum_j 2J\langle S_j \rangle}{k_B T}.
$$
(A2)

Suggest now that there is a slow change of the intensity of the average spins $\langle S_i \rangle$ in the direction [100] so that all spins in any plane (100) are identical. Let z_1 be the number of neighbours in each adjacent layer and z_0 is the number of nearest neighbours in the same plane, so the total number of neighbours is $z = z_0 + 2z_1$. Let now i be the number of (100) planes in the stacking sequence and $m = \langle S_i \rangle/S$. Then the free energy can be written as

$$
\begin{aligned}
F &= -kT\ln Z = N_p S^2 \sum_i J\left[z_0 m_i^2 + z_1 m_i(m_{i+1} + m_{i-1})\right] \\
&\quad - N_p k_B T \sum_i \ln\left(\sum_{n=-S}^{S} \exp \frac{2nJS[z_0 m_i + z_1(m_{i+1} + m_{i-1})]}{k_B T}\right),
\end{aligned}
$$
(A3)

where N_p is the number of ions in a plane. With the approximation $m_{i+1} + m_{i-1} = 2m_i + \frac{d^2 m}{dx^2}|_{x=i}$ we get from (A3), normalizing it to N_p

$$
\begin{aligned}
F &= JS^2 \sum_i \left(zm_i^2 + z_1 m_i \frac{d^2 m}{dx^2}|_{x=i}\right) \\
&\quad - k_B T \sum_i \ln\left(\sum_{n=-S}^{S} \exp \frac{2nJS\left[zm_i + z_1 \frac{d^2 m}{dx^2}|_{x=i}\right]}{k_B T}\right).
\end{aligned}
$$
(A4)

Summarizing the geometrical progression in (A4), we obtain

$$F = JS^2 \sum_i \left(zm_i^2 + z_1 m_i \frac{d^2 m}{dx^2} \big|_{x=i} \right)$$

$$- k_B T \sum_i \ln \left(\frac{sh \left\{ (2S+1)JS \left(zm_i + z_1 \frac{d^2 m}{dx^2} \big|_{x=i} \right) \big/ k_B T \right\}}{sh \left\{ zJS \left(m_i + z_1 \frac{d^2 m}{dx^2} \big|_{x=i} \right) \big/ k_B T \right\}} \right) \tag{A5}$$

The expansion of the second term of (A5) into series at $\frac{z_1}{z} \frac{d^2 m}{dx^2} / k_B T$ gives

$$F = zJS^2 \sum_i \left(m_i^2 + \frac{z_1}{z} m_i \frac{d^2 m}{dx^2} \big|_{x=i} \right)$$

$$- k_B T \sum_i \ln \left(\frac{sh \left\{ (2S+1)zJSm_i / k_B T \right\}}{sh \left\{ zJSm_i / k_B T \right\}} \right)$$

$$- JS \left[Sm_i + \coth \frac{JSzm_i}{k_B T} - (1+2S)\coth \frac{JS(1+2S)zm_i}{k_B T} \right]$$

$$\times z_1 \frac{d^2 m}{dx^2}. \tag{A6}$$

Now, expanding (A6) into series at m up to fourth degree but omitting the term $\frac{z_1}{z} m^3 \frac{d^2 m}{dx^2} / k_B T$ as the nest degree of smallness, obtain

$$F = zJS^2 \left[1 - \frac{2JS(1+S)z}{3k_B T} \right] \sum_i m_i^2$$

$$+ \frac{2J^4 S^5 z^4 (1+S)[1+2S(1+S)]}{45(k_B T)^3} \sum_i m_i^4$$

$$- z_1 JS^2 \left[1 - \frac{4JS(1+S)z}{3k_B T} \right] \sum_i m_i \frac{d^2 m}{dx^2}. \tag{A7}$$

From (A7) follows the well-known expression for the Curie temperature that is

$$k_B T_c = \frac{2JS(1+S)z}{3}. \tag{A8}$$

Substituting $m \frac{d^2 m}{dx^2}$ by $\frac{d}{dx} \left(m \frac{dm}{dx} \right) - \left(\frac{dm}{dx} \right)^2$ and noting that $\sum_i \frac{d}{dx} \left(m \frac{dm}{dx} \right)|_{x=i} = 0$, due to the symmetry requirement, we obtain from (A7), (A8) the free energy per an ion

$$\frac{F}{k_B T_c} = - \frac{3St}{2(1+S)} m^2 + \frac{9S[1+2S(1+S)]}{40(1+S)^3} m^4$$

$$+ \frac{3S}{2(1+S)} \frac{z_1}{z} JS^2 \left(\frac{dm}{dx} \right)^2, \tag{A9}$$

which is a particular form of the GL equation.

For coarse grains (bulk material) the role of surface is neglected and all ions can be considered identical, their magnetization m is constant. Then the condition of minimum of F_{mf} in relation to m gives

$$m = B_s \left[\frac{3Sm}{2(1+S)} \frac{T_c}{T} \right], \tag{A10}$$

where B_s is the Brilluoin function.

For the case of nanoparticles when the surface effects are important, the spins are not identical due to the dependence of the intensity of magnetization from the position. Then the order parameter of ith ion can be represented by the obvious generalization of (A10)

$$m_i = B_s \left[\frac{3S \sum_j m_j}{2z(1+S)} \frac{T_c}{T} \right], \tag{A11}$$

where the summation is performed over the nearest neighbours of the ith ion.